Available online at www.sciencedirect.com
ScienceDirect
International Journal of Heat and Fluid Flow 28 (2007) 44–53
International Journal of HEAT AND FLUID FLOW
www.elsevier.com/locate/ijhff

On the out-of-plane divergence of streamtubes in planar mini-scale flow focusing devices

P.A. Walsh *, E.J. Walsh, M.R.D. Davies

Stokes Research Institute, University of Limerick, Plassey Technological Park, Limerick, Ireland

Accepted 3 May 2006
Available online 17 August 2006

Abstract

In this paper, criteria for the prediction of a 3-D divergence of streamtubes within the entrance region of developing laminar flows between merging streams is presented. This divergence has a direct impact on the application of microscale flow cytometers based upon a 2-D design, as the exact downstream position of the sample population may not be accurately predictable. Also, the phenomenon could adversely affect the efficiency of fluidic sorting systems that have been incorporated into such devices. In this study a mini-scale flow cytometer with three streams merging at a single junction is analyzed to investigate the existence of any three-dimensional divergence of the inlet streams. This is achieved by visualizing dyed inlet streams from both isometric and planar views. A theory to predict this phenomenon is presented and validated using flow visualization and Particle Image Velocimetry (PIV). It is noted that the Reynolds numbers of the inlet streams are the only characterizing parameters for such a device under isothermal pressure driven flow conditions. A range of inlet flow ratios from 1 to 10 between the merging streams are examined. These flow ratio observations were carried out over a Reynolds number range of 23–53. The results show that a three-dimensional divergence of the inlet streams exists within the entrance region. The divergence was found to be almost non-existent at flow ratios of unity but becomes more apparent as the flow ratio is increased. It was also observed that the higher the magnitude of the Reynolds number, the more apparent the divergence became for each flow ratio investigated. Finally, the effect of this phenomenon on the development of microfluidic devices incorporating a similar geometry is discussed and conclusions are drawn.

Keywords: Microfluidics; Flow cytometry; Hydrodynamic focusing; Three-dimensional effects; Entrance region; Developing flows

1. Introduction

Over the past decade, the study of microfluidics has received much attention in the literature. Most of this research has been aimed at developing micro Total Analysis Systems (μTAS) that can be used to increase the efficiency of current macroscale systems. One such field of research that has excelled particularly well in this task is the miniaturization of many clinical diagnostic techniques onto a single microchip (Lab-on-a-Chip Technologies). Toner and Irimia (2005), Schasfoort (2004), Erickson and Li (2004), Yang et al. (2002) and Huh et al. (2005) have all published extensive reviews on different aspects of Lab-on-a-Chip technologies.

In these reviews, probably the most commonly cited requirement is to examine sample populations in detail (e.g. particles, droplets, cells, DNA, etc.). This is usually achieved with the use of optical sensors which require the sample stream to be stretched out into a thin plane for detailed observation. This concept of stretching out the sample population for analysis has been used extensively over the past few decades and is commonly referred to as either hydrodynamic focusing (Wu and Nguyen, 2005) or flow cytometry (Givan, 2001). However, the original design of flow cytometers were axisymmetric where a high gauge blunt needle is placed concentrically within a glass capillary tube. The samples are then injected through the needle and

* Corresponding author. Tel.: +353 61 233716; fax: +353 61 202393.
E-mail address: pat.walsh@ul.ie (P.A. Walsh).

0142-727X/$ - see front matter © 2006 Elsevier Inc. All rights reserved.
doi:10.1016/j.ijheatfluidflow.2006.05.006

Nomenclature

d_h	hydraulic diameter (m)
D	mass diffusion coefficient (m s^{-2})
l_e	entrance length (m)
P	pressure (Pa)
Pe	Peclet number – $(Re)(Sc)$
Re	Reynolds number – $\rho\bar{u}_2 d_h/\mu$
Sc	Schmidt number – $\mu/\rho D$
u	x-component of velocity vector (m s^{-1})
$\bar{u}$	average x-component of velocity vector (m s^{-1})
v	y-component of velocity vector (m s^{-1})
x	streamwise co-ordinate (m)
y	normal to streamwise co-ordinate (m)
u	streamwise velocity component (m s^{-1})

Subscripts

1	relates to the sample population
2	relates to the sample stream
3	relates to sheath streams
T	relates to the total value
S	relates to the static value

Superscript

*	non-dimensional parameter

Greeks

Δ	change in variable
μ	dynamic viscosity (kg m^{-1} s^{-1})
ρ	density (kg m^{-3})

hydrodynamic focusing occurs due to the sheath flow in the glass capillary. The miniaturization of this technique to the microscale has resulted in adapting this design to more simplified two-dimensional geometries. This simplification of the geometry results from limitations in fabrication capabilities and could also be responsible for some unusual flow characteristics encountered within the entrance region of such planar flow cytometers. Flow characteristics in the entrance region are generally not well understood (Sadri and Floryan, 2002), as the majority of analyses consider only fully developed flow conditions.

An important characteristic of all flow cytometers is the ability to accurately predict the downstream position of samples. This accurate positioning is important, as in many μTAS applications of this type, samples are either counted or analyzed by optical instrumentation (Tan et al., 2004; Lin and Lee, 2003). Also, many modern flow cytometers are incorporating fluidic switching mechanisms (Tan et al., 2004; Wang et al., 2005; Lee et al., 2005) so that samples can be sorted according to specified criteria (e.g. size, colour, orientation, etc.). Hence, it is clear that any instabilities or unpredicted divergence of streamtubes encountered could adversely affect the efficient operation of such sorting or detection devices.

In this paper, a planar mini-scale hydrodynamic focusing device, consisting of three streams merging at a single junction (see Figs. 1 and 4) is analyzed in order to investigate flow characteristics within the entrance region that may result from the modified two-dimensional geometry of these devices. The main flow characteristic of interest is a three-dimensional divergence of the inlet streams. Observation of this divergence is attempted by visualizing dyed inlet streams which can be observed from both planar and isometric views due to the scale of the device investigated. Typically in microscale flow cytometry devices, the three-dimensional profile of the sample stream cannot be visualized without the use of confocal microscopy. Hence, there are very few studies on three-dimensional flow characteristics within these hydrodynamic focusing devices.

Simonnet and Groisman (2005) and Chung et al. (2003) are amongst the few authors that carried out similar studies using this technique in microscale flow cytometry devices. However, the objective of these studies was not to look at flow characteristics within the entrance region, but rather to analyze the three-dimensional shape of the sample stream within the fully developed channel. Whilst some of the shapes reported resemble those encountered in the cur-

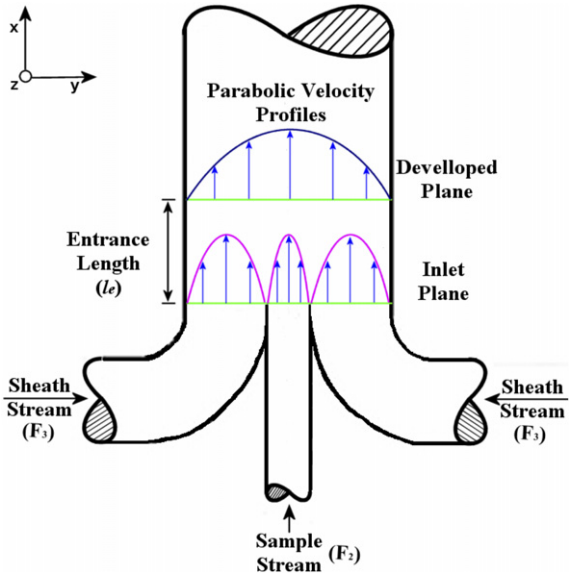

Fig. 1. Schematic outlining velocity profiles at the inlet and developed planes. Fluid streams enter in the directions indicated with viscosity, μ, and density, ρ.

rent study, no reference was made to any three-dimensional divergence of the inlet streams. Both of these studies focused on the creeping flow regime, Reynolds number (Re) $\ll 1$, where viscous forces are known to dominate. In this flow regime, the path of streamlines has been reported by numerous authors (White, 1991; Schlichting, 1979) to be governed by the simple model of Hagen–Poiseuille flow theory. To the authors knowledge very little research has been focused on the range of Re from 1 to 60. This range of Re is of interest, as the further development of these devices implies higher throughputs resulting in either higher operating Re or a further reduction in their physical scale. In this paper, it is attempted to address this short fall by reporting on experiments carried out in this Re range within the geometry considered.

The primary objective of the current study is to investigate both experimentally and theoretically, any three-dimensional flow divergence effects encountered within the entrance region of the fluidic junction. A theory to explain this divergence is put forward and is based upon the simple Hagen–Poiseuille laminar flow model. The validity of this model is first established using PIV measurements. Following this, observations from flow visualization experiments are used to examine any out of plane divergence of the inlet streams within the entrance region. Finally, the consequences of the phenomenon encountered in this paper, on general flow cytometers incorporating planar designs is discussed and conclusions are drawn.

2. Theory

The flow field studied in this analysis is best described by the steady, incompressible, isothermal Navier–Stokes equations for mass and momentum conservation. The characterizing parameters for such a flow field emerge from a dimensional analysis of these governing equations. Such an analysis has been shown to yield the Reynolds number of the inlet streams as the primary characterizing parameters for similar systems (Walsh et al., 2005). Therefore, the fluidic junction under investigation will be characterized in terms of the Re of both inlet streams. These Reynolds numbers will be calculated using both the hydraulic diameter and mean fluid velocity of each inlet port along with the relevant fluid properties.

Throughout this paper the sheath streams entering the fluidic junction from the side ports are termed 'F_3' streams while the center stream is termed the 'F_2' stream, see Fig. 1. The unreferenced 'F_1' stream is to consist of the samples to be analyzed. This stream generally consists of a different phase, such as solid particles or droplets, and enters the fluidic junction embedded within the F_2 stream. These samples are assumed to be neutrally buoyant within this stream and so will follow the path of the F_2 streamlines.

In order to better understand the momentum mixing process between the merging streams, a quasi-three-dimensional analysis of flow theory for the fluidic junction is presented in terms of momentum transfer between streamlines through viscous interaction. This is achieved by first discussing the two-dimensional case, (x, y), and then extending the analysis into the third dimension, (z). The purpose of this is to attempt to explain any tendency for a three-dimensional divergence of streamlines within the entrance region.

It has been reported by numerous authors (Holman, 1986; Bejan, 1993 White, 1994) that bounded channel flows with Reynolds numbers of order unity experience a highly viscous flow regime and that the velocity profiles between the bounding surfaces are strictly governed by the well established Hagen–Poiseuille flow theory. In Fig. 1, a schematic of such a laminar flow regime in the two-dimensional geometry considered is presented. It is assumed that the velocity profiles at the inlet plane for each of the 'F_2' and 'F_3' fluids are governed by Eq. (1), where 'Y' is the distance between the bounding surfaces.

$$u_y = u_{\max}\left(1 - \left(\frac{y}{Y}\right)^2\right) \tag{1}$$

Also, at a second plane some distance downstream of the inlet plane, the flow will fully develop into another parabolic velocity profile. This distance is commonly referred to as the entrance length of the channel and is usually in the order of microns for creeping flows ($Re < 1$) (Curtin et al., 2003). The magnitude of the entrance length can be estimated from empirical correlations reported in the literature. However, these are generally reported for developing flow into a single channel from a large reservoir. A well accepted correlation reported both by White (1991) and Schlichting (1979) predicts the entrance length for viscous laminar flows to be $l_e/d_h \approx 0.06 \times Re_h$.

Manipulating the mass conservation equation for steady, isothermal and incompressible flow; the divergence of streamlines across the width of the channel can be obtained. This is achieved by calculating the change in local position across the channel width, which is required to maintain a constant flow rate whilst the velocity profile develops from the inlet to the developed plane. The resulting divergence of streamlines due to the development of a downstream parabolic velocity profile is shown in Fig. 2 across the right half of the channel width for two flow ratios ($u^* = \bar{u}_3/\bar{u}_2$) of (a) 1 and (b) 10. Accelerating and decelerating streamlines are marked by dashed red and blue lines, respectively.[1] The overall effect of this to an observer of a 2-D flow field is that the 'F_2' stream would be seen to diverge into a thicker or thinner stream in the downstream channel, with the degree of divergence being dependant upon the ratio of the inlet velocities.

If it is assumed that the entrance length is small, then it is also reasonable to take, as a first approximation, the assumption that the total pressure drop over this length is negligible, Eq. (2).

[1] For interpretation of the references in colour in figures, the reader is referred to the Web version of this article.

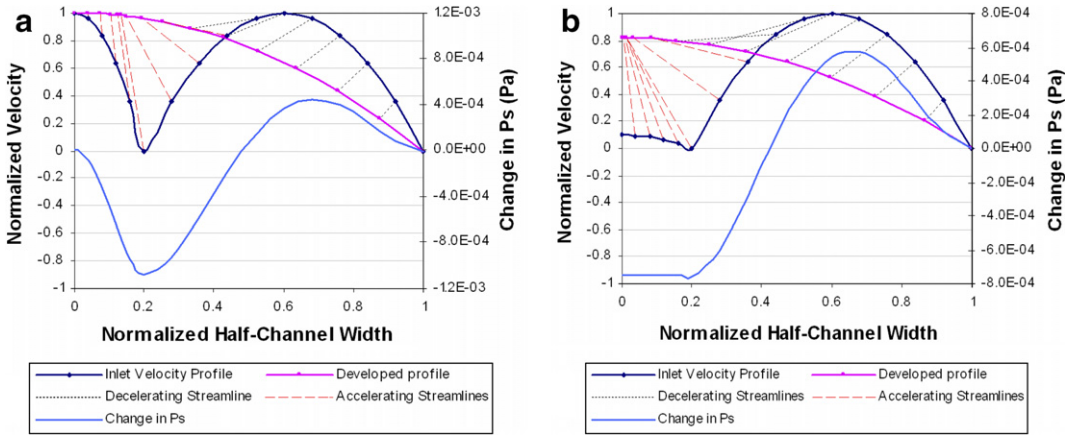

Fig. 2. Plot of inlet and developed velocity profiles indicating the divergence of streamlines for (a) $u^* = 1$ and (b) $u^* = 10$. Also indicated on a secondary axis is the required change in local static pressure across the channel width at the inlet plane.

$$
\begin{aligned}
&P_{T_{\text{Inlet}}} \approx P_{T_{\text{Developed}}} \\
&\quad \Rightarrow (P_{S,y} + 1/2\ \rho u_y^2)_{\text{Inlet}} = (P_{S,y} + 1/2\ \rho u_y^2)_{\text{Developed}} \qquad (2) \\
&\quad \Rightarrow \Delta P_{S,y} = 1/2\ \rho (u^2_{y,\text{Developed}} - u^2_{y,\text{Inlet}})
\end{aligned}
$$

Since the total pressure is equal to the sum of the static and dynamic pressures, an expression can now be derived for the change in local static pressure due to the acceleration or deceleration of streamlines within the entrance region, Eq. (2). The required variations in local static pressure for the flow in the downstream channel to fully develop can now be calculated and is presented in Fig. 2 on a secondary axis. The effect of this pressure gradient across the channel width is to cause streamlines to deviate in the directions indicated in Fig. 2. This is caused by an equalizing of static pressure across the channel width as, if any variations were to exist in the fully developed plane, parallel streamlines would not be observed. It is seen for the case when u^* equals unity, that there are two high local static pressure regions which almost balance each other out in the entrance region. The effect of this is that there is little divergence of F_2 streamlines. However, when the flow ratio is increased to 10, it can be seen that there is only one static pressure peak. The fluid then flows from the areas of high to low pressure in order to achieve equilibrium and hence, a fully developed profile.

Another interesting point that can be noted from this analysis is that the area underneath the static pressure curve represents the work done by the fluid as it flows through the junction. In the current analysis, when the flow ratio is a minimum of unity, the average change in static pressure is always negative. This represents a pressure drop at the fluidic junction. However it can be shown that, as the flow ratio decreases, the average static pressure changes to a positive value. At this point, the fluidic junction will generate a pressure rise and hence could be used as an injector pump in the same manner as that described by Bird et al. (2002) for turbulent flows.

The next step of the analysis is to apply the same theoretical argument to the third dimension, (z). This is achieved by assuming a parabolic velocity profile through the depth of the channel. The effect of this is to generate a parabolic local static pressure variation through the channel depth, with the maximum values of the profile at the channel mid-depth. These values correspond to those presented in the 2-D analysis described. The profiles corresponding to the flow ratios shown in Fig. 2 are presented

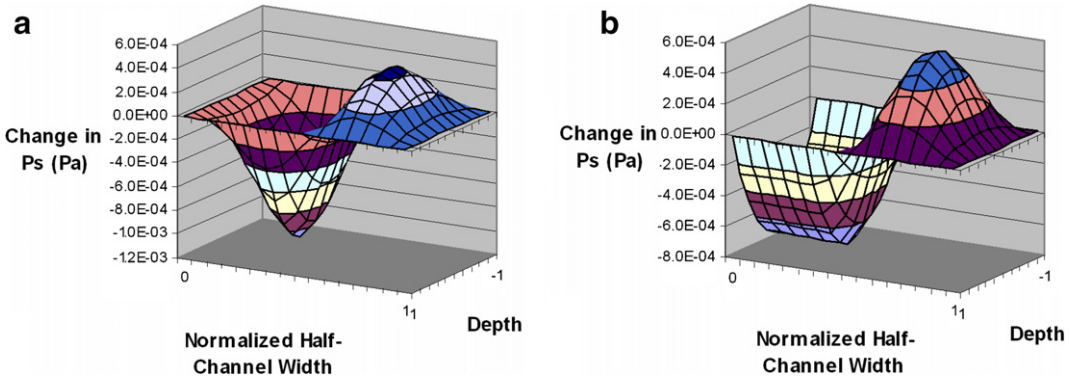

Fig. 3. Three-dimensional plot of the change in static pressure on the inlet plane required to allow the flow to fully develop in the downstream channel. Profiles are shown for (a) $u^* = 1$ and (b) $u^* = 10$ corresponding to those in Fig. 2.

on the 3-D plots of Fig. 3(a) and (b). The front and back planes of these plots correspond to the top and bottom bounding surfaces of the channel while the left and right planes correspond to the symmetry plane and the right side of the channel wall. It can be seen that the maximum pressure variation in the inlet plane exists at the mid-depth of the channel and that this pressure variation gradually decreases towards zero at the top and bottom bounding surfaces. In Fig. 3(a), when $u^* = 1$, the effect at the mid-depth of the channel would be to converge streamtubes slightly towards the symmetry plane as predicted by the 2-D analysis. However, looking at the pressure variation across the channel width moving closer to the top and bottom bounding surfaces, it is seen that the change in static pressure decreases gradually and is uniformly zero at the top and bottom surfaces. This has the effect of forcing F_3 streamtubes at the mid-depth of the channel to converge more towards the symmetry plane compared to those adjacent to the top and bottom bounding surfaces.

This effect is amplified when the flow ratio between the streams is increased to 10 as shown in Fig. 3(b). Now severe necking occurs at the mid-depth of the channel and the degree of necking reduces towards the upper and lower surfaces of the channel. The overall effect of this phenomenon on the F_2 fluid is that it will be forced to converge towards the symmetry plane much more at the mid-depth x–y plane than at parallel planes adjacent to the top and bottom bounding surfaces. Such a characteristic of developing laminar flows between merging streams should result in the width of the F_2 stream changing through the channel depth and could theoretically promote some out of plane motion of streamtubes within the entrance region when u^* values are much greater than unity.

3. Experimentation

Two experimental methods are described; these are flow visualization and Particle Image Velocimetry (PIV). Both of these methods were used in an attempt to validate the theory presented. For both techniques, the design of the fluidic junction is shown in the rendered drawing and photograph of Fig. 4. The fluidic junction was manufactured from Perspex and the dimensions of the channels are 4×4 mm for the F_2 ports and 4×8 mm for the F_3 ports. The length of the test section where the two streams are in contact is 40 mm. This scale was chosen to simplify both manufacturing and experimental measurement. Also, since scaled results are to be produced, they can be applied to both small and large scale models of a similar geometry.

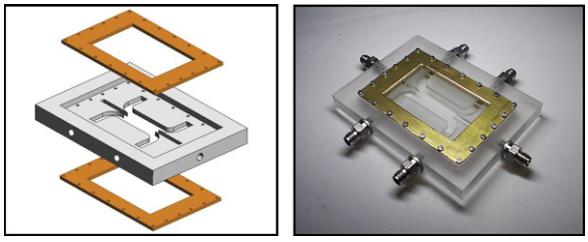

Fig. 4. Rendered drawing and photograph of scaled up test piece manufactured to investigate the entrance effects of interest.

3.1. Flow visualization set-up

A schematic of the experimental set-up for capturing flow visualization images is presented in Fig. 5. Characterization of the flow field requires that the boundary conditions be accurately controllable. For this reason, high precision positive displacement gear and syringe pumps are used to pump the F_3 and F_2 fluids, respectively so that their flow rates can be measured accurately. There is also a second syringe pump extracting fluid from the F_2 exit port. This is to ensure that the inlet and exit flow rates of both the F_2 and F_3 streams are equal.

For both sets of experiments, water was used as the working fluid. However, for the series of flow visualization experiments, both fluid streams were dyed using a 0.8% volume mix of artificial colouring so that the flow architecture could be clearly visualized. The F_2 stream was dyed orange (bright shade) while the F_3 streams were dyed blue (dark shade),[1] both fluids were dyed using the same dye concentration to eliminate any possible buoyancy mismatch due to the addition of the dye. Finally, the device was back illuminated using a diffuse white light illumination source and flow visualization images were recorded using a 1.2 Mega pixel Sony colour CCD camera (DFW-SX900).

Also of significance in the current study is the Peclet number (Pe) of the flow. This dimensionless parameter provides a measure of the ratio between advection and mass diffusion in the flow field and is defined by the product of the Reynolds number and the Schmidt number (Sc) of the flow. Since the mass diffusion coefficient between liquid–liquid streams is typically of the order 10^{-9} m^2/s

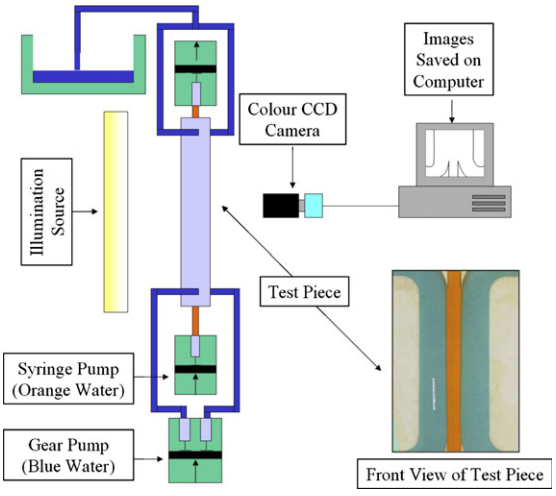

Fig. 5. Schematic of experimental set-up for flow visualization experiments with front elevation photo of the test piece included (available in colour online).

(Bird et al., 2002), the Schmidt number of the flow is of order 10^3. Hence, the lowest Peclet number anticipated for the range of operating conditions considered is approximately 10^4. Such a high value for this parameter suggests that the dominant mixing mode in the fluidic device under investigation will be by advection. In fact, it is anticipated that the maximum length scale for which blurring of the interface could occur due to mass diffusion alone in the current study is less than 1 μm. This length is calculated using the diffusion coefficient stated and a minimum flow velocity of 0.002 m s^{-1} through the 40 mm length of downstream channel. Hence, mass diffusion should not be apparent in the scale of device investigated herein.

3.2. Particle Image Velocimetry set-up

A labeled photograph of the apparatus set-up for obtaining Particle Image Velocimetry (PIV) results is presented in Fig. 6(top). It is seen that the boundary conditions are controlled using the same pumps as were used for the flow visualization set-up. A macroscale PIV set-up is used where a thin laser sheet of 1 mm thickness is obtained using a fiber optic laser sheet generator to deliver light from Nd–YAG double pulsed lasers. The schematic of Fig. 6(left) depicts the modification to the fluidic junction required for the introduction of the laser sheet. The laser sheet was aligned at the channel mid-depth and occupied 25% of the total channel depth. Hence, according to Eq. (1), there is a maximum of a 2% variation in the velocities encountered within the depth of this plane. A TSI Powerview Plus straddle frame CCD camera was orientated perpendicular to the illumination plane and used to acquire image pairs for analysis with a 60 mm focal length lens. A software user interface also obtained from TSI and called 'Insight 3G' is used throughout experimentation for: synchronizing the camera and lasers; recording image pairs; cross-correlating image pairs; and finally applying some validation criteria to the results obtained.

The seeding particles used consisted of 8–12 μm diameter silver coated hollow glass spheres. These seeding particles have a specific gravity of 1.1 g/cm^3 and were almost neutrally buoyant within the working fluid. A nyquist grid engine was used for cross-correlation of image pairs recorded with 32×32 interrogation regions overlapped by 50% to account for particles that travel from one interrogation region to another between consecutive images. A much more detailed discussion on this cross-correlation procedure and on the PIV technique itself is presented by Raffel (1998).

4. Results and discussion

In this section, the results obtained from the series of flow visualization and PIV experiments outlined are presented and discussed. The flow architecture observed from flow visualization images obtained whilst varying the flow ratio is first described. PIV results are then presented to describe the developing profiles for the two cases considered theoretically of u^* equal to 1 and 10. This is followed by reporting on a three-dimensional divergence of the inlet streams observed during experimentation. The effect of changing the operational Reynolds number, Re_3, on this phenomenon is then investigated and the results are com-

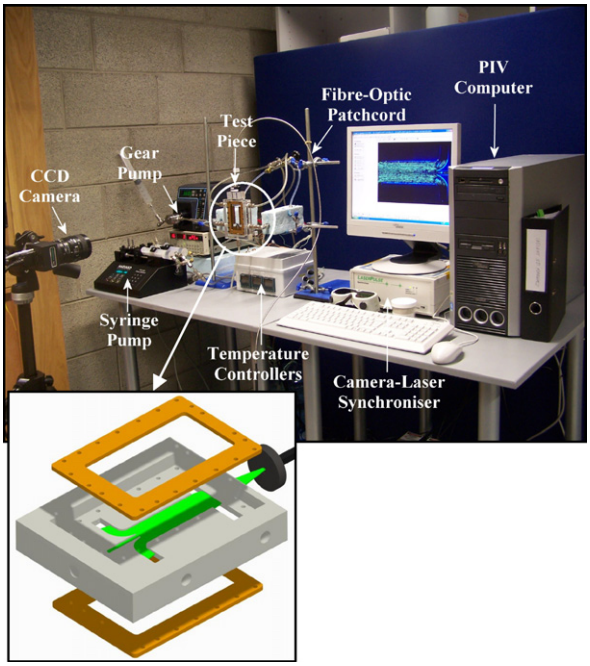

Fig. 6. Labeled photograph of apparatus set-up (top) in the laboratory for obtaining full-field Particle Image Velocimetry (PIV) results. Also shown (left) is a drawing of the modified fluidic junction manufactured to incorporate the laser sheet.

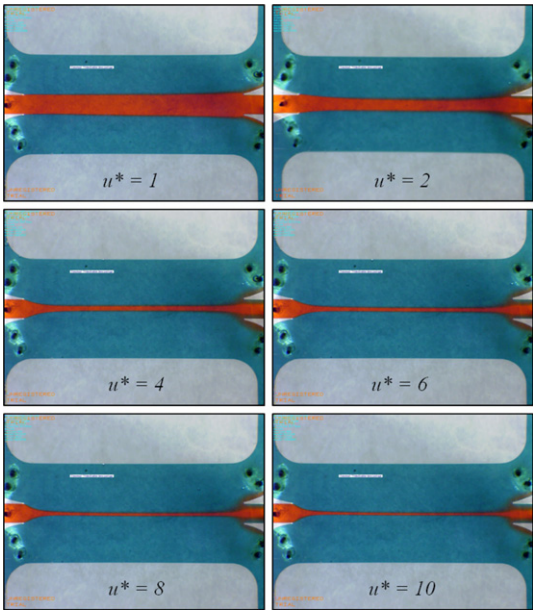

Fig. 7. Flow visualization images outlining the effect of varying the velocity ratio (u^*) between the F_2 and F_3 inlet streams. $Re_3 = 28$ throughout; Re_2 varied between 21 and 2.1; all streams flow from left-to-right (available in colour online).

pared to the theory presented. Finally, the impact of this phenomenon in flow cytometry or hydrodynamic focusing devices is commented upon.

Flow visualization results are presented over a velocity ratio, $u^* = \bar{u}_3/\bar{u}_2$, range of 1–10 between the merging streams in Fig. 7. It is seen that a laminar flow regime exists, as the path of the streamlines at the interface between the merging streams is well defined. The flow field was also observed to be steady so that the instantaneous images presented accurately portray the time averaged flow architecture. In Fig. 7, Re_3 was held constant at 28 throughout and Re_2 was varied from 21 to 2.1 to obtain flow ratios between 1 and 10, respectively. The result observed, is that the sample stream converges as expected for set velocity ratios. It is seen that when the velocity ratio is large the F_2 stream is stretched into a very thin thread when flowing through the device. Alternatively, when the velocity ratio is of order unity, the F_2 stream remains at approximately constant thickness. These observations agree well with the general conclusions drawn from the simple two-dimensional theory presented.

During experimentation, velocity profiles across the channel width were measured using PIV at a number of planes along the channel length (x-direction). These profiles were normalized using the maximum downstream velocity and are presented at an operational Re_3 of 33 for u^* values of 1 and 10 in Fig. 8(a) and (b), respectively. In these plots, normalized velocity profiles at planes a distance of 1, 3, 5, 7, 13 and 21 mm downstream of the merging plane are presented for each flow ratio. The velocity profile directly at the merging plane (0 mm) was not attainable during experimentation due to reflections from the channel walls. However, it is apparent that similar velocity profiles to those assumed in the theory presented exist for the flow regime considered. It is seen for the case when u^* equals unity that both streams enter at approximately the same inlet velocity and that the fluid at the interface between the two streams is accelerated in the streamwise direction. This acceleration is seen to continue until the flow becomes almost fully developed at a distance of approximately 7 mm downstream of the merging plane. This is apparent, as the profiles presented at distances of 7, 13 and 21 mm are almost identical. For the case of u^* equal to 10, it is seen that this time the whole of the F_2 stream is accelerated in the streamwise direction and that fluid flows from the F_3 stream towards the centerline of the channel as the profile develops. This time the entrance length is seen to be approximately 13 mm. These measured entrance lengths are found to differ considerably to those proposed by White (1991) and Schlichting (1979) for simple pipe flow. It was found that when u^* was equal to unity, the entrance length was only 60% of that predicted, however when u^* was equal to 10, the entrance length increased to 140% of that predicted. These differences are not surprising given the differences in both the geometry and inlet conditions considered in this study compared to those for which the correlation was empirically determined.

Referring back to the flow visualization images presented in Fig. 7, it is apparent that when u^* is equal to unity the concentration of the streams entering through each port is equal to that exiting through the corresponding ports. This is an expected result, as it is seen in Fig. 5 that an infuse/withdraw syringe pump was used to both infuse and withdraw the sample stream at the same flow rate. Hence, it is expected that the entire sample stream entering the fluidic junction exits through the corresponding F_2 exit port. An interesting phenomenon is observed however when the flow ratio increases. This is the fact that some of the F_2 stream exits through the F_3 exit ports and visa versa. This phenomenon becomes more obvious for the larger flow ratios considered and appears as mass diffusion between the merging streams from the planar views presented. It should be noted that a similar phenomenon resulting from mass diffusion alone has been reported in microscale literature and is referred to as the 'Butterfly Effect' (Kamholz et al., 1999). However, since the Butterfly Effect is a phenomenon that is associated with mass diffusion and it has been stated that the length scale anticipated

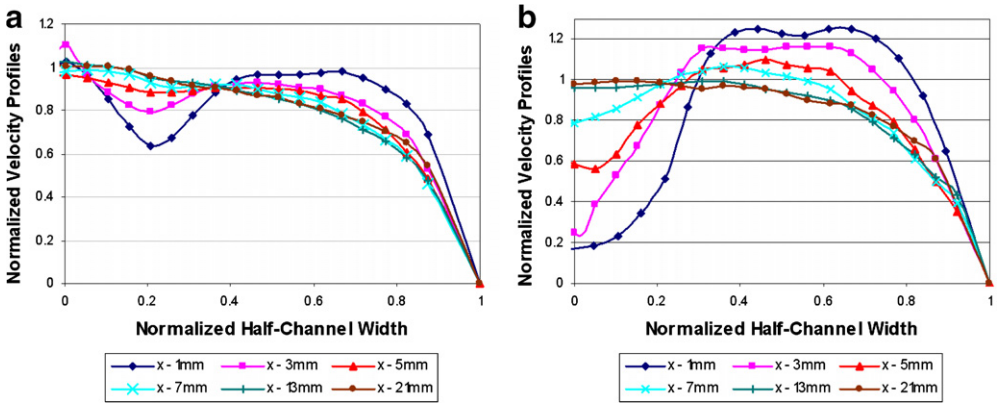

Fig. 8. Normalized velocity profiles obtained using Particle Image Velocimetry (PIV) of developing boundary layers between the merging streams for (a) $u^* = 1$ and (b) $u^* = 10$. Normalized velocity profiles are superimposed on each plot for six different planes downstream of the merging plane.

for this transfer process in the high Peclet number flows encountered is of the order 1 μm, it is believed that this phenomenon is not likely to be observed in the current study. Instead it is believed that a more likely explanation for the observed phenomenon is the 3-D divergence of the inlet streams that was considered in the theory section. For this reason, it was decided to attempt to observe the anticipated 3-D divergence of streamtubes by looking closely at the entrance region of the channel from an isometric view.

One such isometric view is presented in Fig. 9, the boundary conditions for the image displayed are $Re_3 = 53$ and $u^* = 10$. This image serves to illustrate the structure of the F_2 stream through the depth of the channel. It is clear that in the developed flow the intensity of the F_2 stream is greatest nearer the top and bottom bounding surfaces. This indicates that there is a thicker layer of the F_2 stream adjacent to these surfaces than at the mid-depth of the channel and supports the conclusions drawn from the quasi-3-D theory presented. The result of this is that the expected shape of the F_2 stream through the depth of the channel would be similar to that presented in Fig. 9(c). It is worth noting at this point, that this type of structure for the sample stream has also been observed by both Simonnet and Groisman (2005) and Chung et al. (2003) within similar microscale flow focusing devices using confocal microscopy. However, if such a structure were to exist without any 3-D divergence of the inlet streams, it would be observed from a planar view that the reverse would occur in the symmetric exit region of the device considered. This would result in all of the inlet streams exiting through their respective ports and is seen not to be the case when the flow ratio is greater than unity. Hence, some degree of 3-D flow must exist within the entrance region causing the F_2 stream to separate towards the top and bottom bounding surfaces, as is indicated in Fig. 9(b). Furthermore, the 'mass diffusion' like nature of this phenomenon when viewed from planar images provides a simple method to quantify the extent of the 3-D divergence. This is achieved by comparing the dye concentration of the F_2 exit stream to that of the F_2 inlet stream. The effect of varying the boundary conditions may also be examined in this manner.

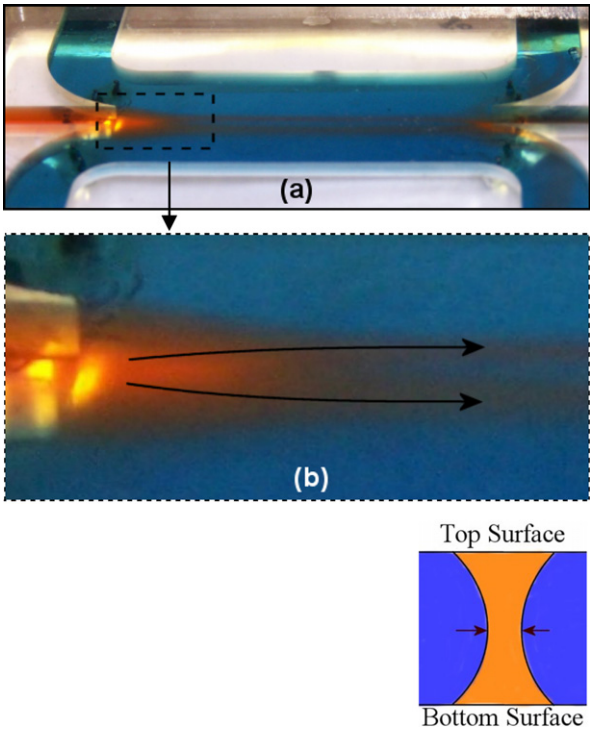

Fig. 9. Isometric flow visualization image recorded depicting (a) the overall flow structure observed, (b) separation of the F_2 stream to the top and bottom surfaces within the entrance region and (c) a schematic of the flow structure anticipated through the depth of the channel. Boundary conditions are $Re_3 = 53$ and $u^* = 10$ and flow is from left-to-right (available in colour online).

Another plausible explanation for the 3-D divergence observed could be due to small gaps existing between the channel geometry and the top and bottom bounding surfaces. Such gaps could arise when (a) using gaskets that do not exactly match the channel profile or (b) by a thin layer of sealant creating small voids between the channel geometry and the sealing surfaces. Hrnjak and Tu (2005) have hypostasized that such unknown channel roughness coupled with unknown thickness of the sealant layers may be responsible for the large degree of scatter present in the literature for global pressure measurements in microchannels. In the current study, this characteristic was minimized by sealing the channel using a compression fit alone. Hence, it is believed that this was not the predominant driving force for the 3-D divergence observed in the current study.

In order to determine the effect of changing the operational Reynolds number on the 3-D divergence considered, a parametric study was undertaken to determine the effect of varying both the flow ratio and the value of Re_3 on the flow architecture. These are varied from 1 to 10 and 23 to 53, respectively. This parametric variation is an important consideration, as it outlines the effect of increased operational Reynolds number on the flow structure observed for constant u^* values. This may also give some insight as to whether or not the 3-D divergence observed in the current study will be apparent in a creeping flow regime. The results from this parametric variation are presented in Fig. 10 and examined using the methodology described for comparing planar views. The flow ratio is seen to increase in columns from left to right and the value of Re_3 to increase in rows from top to bottom. The effect of increasing Re_3 is to increase the magnitude of the pressure variation encountered in the entrance region, across the channel width. For this increased pressure variation, the theory predicts that the 3-D phenomenon be more pronounced. This is seen to be the case, as for the maximum flow ratios of 10, it is seen that the concentration of F_2 fluid in the exit port goes from about 85% of the inlet concentration at a Re_3 of 23 to about 50% at a Re_3 of 53. This suggest that a further reduction in Re_3 to the creeping flow regime ($Re_3 \ll 1$) may result in up to 100% of the F_2 stream exiting

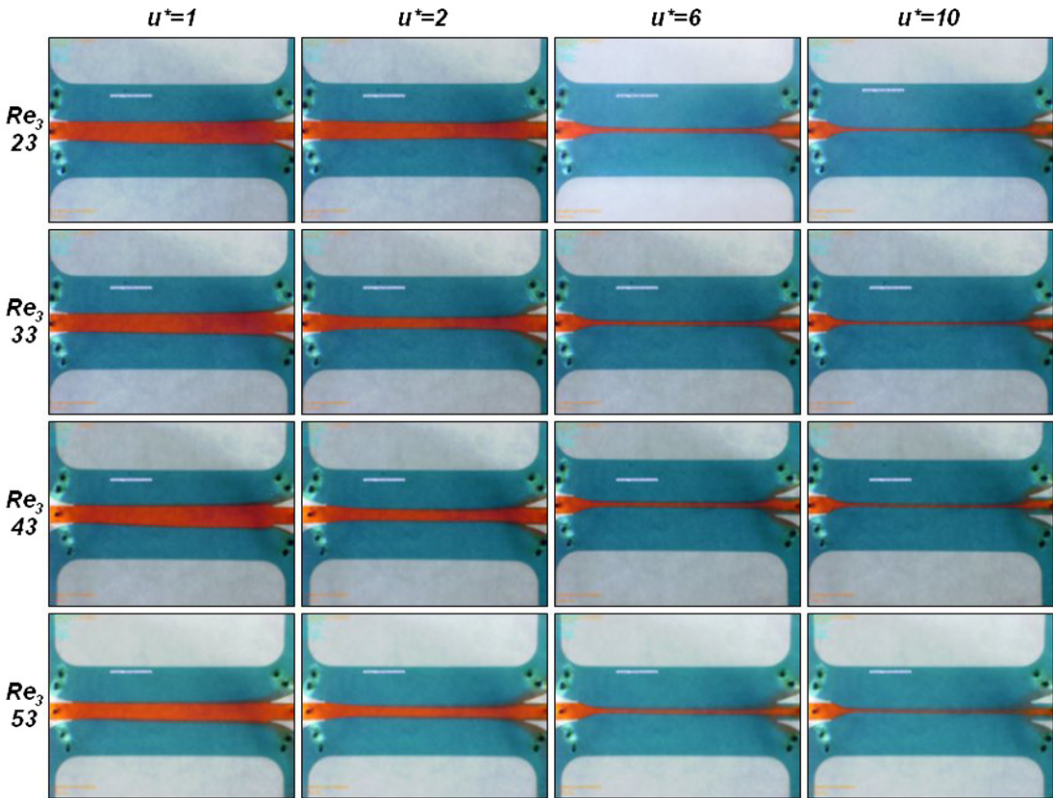

Fig. 10. Flow visualization results obtained from a parametric variation in both Re_3 and u^* to evaluate the extent of 3-D flow phenomenon observed. Flow is from left-to-right in all images, with Re_3 increased from 23 to 53 in rows and u^* from 1 to 10 in columns (available in colour online).

through the correct port, hence eliminating the 3-D divergence encountered in the current study. It is also anticipated from the theory presented, that the 3-D divergence be non-existent when the thickness of the F_2 stream remains constant in the entrance region. This scenario was encountered in the current study for $u^* \sim 1$, where it is observed in Fig. 10 that the concentration of F_2 fluid in the exit port is approximately equal to that in the inlet port and remains unchanged as Re_3 is increased.

From the results presented in this paper it is reasonable to suggest that the phenomenon reported may well be experienced in scaled down geometries operating at the same or lower Reynolds numbers. However, such an observation has not been reported in the literature. This is thought to be due to its 'mass diffusion' like nature between the F_2 and F_3 streams. This means that the phenomenon encountered may be easily mistaken for mass diffusion in down-scaled models as 3-D flow visualization images are not readily attainable without the use of confocal microscopy. Instead 2-D spectral intensity mapping of dyed flows (Curran and Davies, 2004) or Interferometry (Garvey et al., 2004; Walsh and Davies, 2005) are generally used to obtain 2-D concentration measurements averaged through the depth of the fluid layer. Hence, the phenomenon encountered in this paper should be considered in such studies, especially if the operational Reynolds number is of the same order of magnitude as that investigated in the current study.

5. Conclusions

In this paper, a phenomenon encountered in developing laminar velocity profiles between merging streams was both theoretically and experimentally investigated. The main point emerging from the theoretical analysis was that at flow ratios much greater than unity, larger forces exist at the mid-depth of the fluid layer to divert streamtubes towards the centerline of the channel than closer to the top and bottom bounding surfaces. Hence, it was concluded that this could induce some three-dimensional flow characteristics within the entrance region. Subsequently, the analytical solution used to define the velocity profiles in the theory presented was verified using PIV data and flow visualization images were used to verify the existence of the anticipated three-dimensional divergence of streamtubes within the entrance region. The primary characteristics affecting this divergence were seen, as the theory suggested, to be the operational Reynolds number and the flow ratio between the merging streams. It was observed that at a flow ratio of unity, the divergence was negligible throughout whilst at a flow ratio of 10, it was observed that up to 50% of the sample stream exited through incorrect ports. This percentage was seen to reduce considerably upon reducing the operational Reynolds number but did not eliminate the phenomenon within the range of boundary conditions considered. Because of the extent of the divergence

observed at high Re_3 values it is expected that samples embedded in the F_2 stream would move towards the top and bottom bounding surfaces as they enter the downstream channel. This can have an undesired effect on sorting systems based on the principle of fluidic switching, as the samples may leave through incorrect ports just as the F_2 stream did in the current study. It is concluded that a reduction in scale of such flow cytometers may be necessary to advance throughput rates rather than simply increasing flow rates. It is also concluded that the phenomenon reported in the current study may well be experienced in scaled down geometries operating at the same or lower Reynolds numbers but has not been reported in the literature. This is thought to be due to its 'mass diffusion' like nature when viewed using common measurement methods such as, 2-D spectral intensity mapping or Interferometry.

Acknowledgement

The authors would like to acknowledge the financial support of the Irish Research Council for Science, Engineering and Technology (IRCSET).

References

Bejan, A., 1993. Heat Transfer. John Wiley & Sons, Inc., New York.

Bird, R., Warren, E., Edwin, N., 2002. Transport Phenomenon, second ed. Wiley, New York.

Chung, S., Park, S.J., Kim, J.K., Chung, C., Han, D.C., Chang, J.K., 2003. Plastic microchip flow cytometer based on 2- and 3-dimensional hydrodynamic flow focusing. Microsystem Technologies-Micro-and Nanosystems-Information Storage and Processing Systems 9 (8), 525–533.

Curran, K., Davies, M., 2004. Spectral intensity mapping and analysis of dyed microflows. In: Proc. of ASME-ICMM, Rochester, New York, pp. 183–190.

Curtin, D., Newport, D., Davies, M.R., 2003. A comparison of micro-PIV experiments in a mini-channel to numerical and analytical solutions. Thermal Science and Engineering 11 (6), 35–42.

Erickson, D., Li, D.Q., 2004. Integrated microfluidic devices. Analytica Chimica Acta 507 (1), 11–26.

Garvey, J., Newport, D., Dalton, T., 2004. Liquid diffusion measurement in micro/mini-channels from full-field digital Phase Measurement Interferometry. In: Proceedings of ASME-ICMM, Rochester, New York.

Givan, A.L., 2001. Flow Cytometry: First Principles, second ed. Wiley, New York.

Holman, J.P., 1986. Heat Transfer, sixth ed. McGraw-Hill, Inc., New York.

Hrnjak, P., Tu, X., 2005. Single-phase pressure drop in microchannels. In: Proc. of ECI Heat Transfer and Fluid Flow in Microscale, Castlevecchio Pascoli, Italy.

Huh, D., Gu, W., Kamotani, Y., Grotberg, J.B., Takayama, S., 2005. Microfluidics for flow cytometric analysis of cells and particles. Physiological Measurement 26 (3), R73–R98.

Kamholz, A.E., Weigl, B.H., Finlayson, B.A., Yager, P., 1999. Quantitative analysis of molecular interaction in a microfluidic channel: the T-sensor. Analytical Chemistry 71 (23), 5340–5347.

Lee, G.B., Lin, C.H., Chang, S.C., 2005. Micromachine-based multichannel flow cytometers for cell/particle counting and sorting. Journal of Micromechanics and Microengineering 15 (3), 447–454.

Lin, C.H., Lee, G.B., 2003. Micromachined flow cytometers with embedded etched optic fibers for optical detection. Journal of Micromechanics and Microengineering 13 (3), 447–453.

Raffel, M., 1998. Particle Image Velocimetry: A Practical Guide. Springer, New York.

Sadri, R.M., Floryan, J.M., 2002. Accurate evaluation of the loss coefficient and the entrance length of the inlet region of a channel. Journal of Fluids Engineering—Transactions of the ASME 124 (3), 685–693.

Schasfoort, R.B.M., 2004. Proteomics-on-a-chip: the challenge to couple lab-on-a-chip unit operations. Expert Review of Proteomics 1 (1), 123–132.

Schlichting, H., 1979. Boundary Layer Theory, seventh ed. McGraw-Hill, Inc., New York.

Simonnet, C., Groisman, A., 2005. Two-dimensional hydrodynamic focusing in a simple microfluidic device. Applied Physics Letters 87 (11).

Tan, Y.C., Fisher, J.S., Lee, A.I., Cristini, V., Lee, A.P., 2004. Design of microfluidic channel geometries for the control of droplet volume, chemical concentration, and sorting. Lab on A Chip 4 (4), 292–298.

Toner, M., Irimia, D., 2005. Blood-on-a-chip. Annual Review of Biomedical Engineering 7, 77–103.

Walsh, P.A., Davies, M.R.D., 2005. An evaluation of phase measurement interferometry for obtaining full-field temperature measurements in a small scale fluidic junction. In: Proc. of ECI Heat Transfer and Fluid Flow in Microscale, Castlevecchio Pascoli, Italy.

Walsh, P.A., Davies, M.R.D., Dalton, T., 2005. Characterisation of stability criteria for pressure driven flows in small length scale fluidic devices. In: Proc. of ASME Summer Heat Transfer Conference, San Francisco, California, USA.

Wang, M.M., Tu, E., Raymond, D.E., Yang, J.M., Zhang, H.C., Hagen, N., Dees, B., Mercer, E.M., Forster, A.H., Kariv, I., Marchand, P.J., Butler, W.F., 2005. Microfluidic sorting of mammalian cells by optical force switching. Nature Biotechnology 23 (1), 83–87.

White, F.M., 1991. Viscous Fluid Flow, second ed. McGraw-Hill, Inc., New York.

White, F.M., 1994. Fluid Mechanics, third ed. McGraw-Hill, Inc., New York.

Wu, Z.G., Nguyen, N.T., 2005. Hydrodynamic focusing in microchannels under consideration of diffusive dispersion: theories and experiments. Sensors and Actuators B—Chemical 107 (2), 965–974.

Yang, J., Li, C.W., Yang, M.S., 2002. Lab-on-a-chip (microfluidics) technology. Acta Biochimica et Biophysica Sinica 34 (2), 117–123.